Precise Quantization of the Anomalous Hall Effect near Zero Magnetic Field

A. J. Bestwick, E. J. Fox, Xufeng Kou, Lei Pan, Kang L. Wang, and D. Goldhaber-Gordon

Precise quantization of anomalous Hall effect near zero magnetic field

A. J. Bestwick,[1] E. J. Fox,[1] Xufeng Kou,[2] Lei Pan,[2] Kang L. Wang,[2] and D. Goldhaber-Gordon[1, *]

[1]*Department of Physics, Stanford University, Stanford, CA 94305, USA*
[2]*Department of Electrical Engineering, University of California, Los Angeles, CA 90095, USA*
(Dated: March 18, 2015)

We report a nearly ideal quantum anomalous Hall effect in a three-dimensional topological insulator thin film with ferromagnetic doping. Near zero applied magnetic field we measure exact quantization in Hall resistance to within a part per 10,000 and longitudinal resistivity under 1 Ω per square, with chiral edge transport explicitly confirmed by non-local measurements. Deviations from this behavior are found to be caused by thermally activated carriers, as indicated by Arrhenius law temperature dependence. Using the deviations as a thermometer, we demonstrate an unexpected magnetocaloric effect and use it to reach near-perfect quantization by cooling the sample below the dilution refrigerator base temperature in a process approximating adiabatic demagnetization refrigeration.

The discovery of the quantum Hall effect (QHE) [1, 2] led to a new understanding of electronic behavior in which topology plays a central role [3, 4]. Initially, the critical experimental observation was the precise quantization of the Hall resistance to integer divisions of h/e^2, where h is Planck's constant and e is the electron charge. This quantization, immune to sample-specific disorder, now forms the basis for a metrological standard [5]. A complementary feature—zero longitudinal resistance, reflecting resistanceless transport along sample edges—could also have technological applications, were it not for the demanding environmental requirements for achieving the QHE: a large magnetic field to break time-reversal symmetry (TRS) and, in most cases, cryogenic temperatures. Ideas for producing a similar phenomenology without an external magnetic field have long been considered [6], often involving the interplay of symmetry and topology in new material systems.

In the past decade, topological insulators (TIs) have emerged as a promising approach. In both two-dimensional [7–9] and three-dimensional [10–14] forms, conduction in TIs is restricted to topologically-protected boundary states. In the 3D case, the presence of ferromagnetic exchange can break TRS, opening a gap in the otherwise Dirac-like surface states [15–17]. But topology adds a twist: even a uniformly magnetized sample will have, relative to the normal vector of the surface, a domain boundary where the magnetization switches from inward to outward. Along this line the gap should close, restoring conduction [16]. In a thin film geometry in which the easy axis of the magnetism is out-of-plane, confinement along the sample side wall should ensure conduction is one-dimensional while the surface gradient of the magnetism restricts it to only one direction, leading to ballistic, chiral transport. In a Hall bar geometry, this would be observed as the quantum anomalous Hall effect (QAHE), with a zero longitudinal resistance and a transverse resistance quantized to h/ne^2, where n is typically ± 1 but can in principle be a higher integer given sufficiently strong exchange [18].

Experimental realization of the QAHE has been swift. Doping films of the ternary TI family $(Bi,Sb)_2Te_3$ with Mn or Cr was found to produce robust out-of-plane ferromagnetism and a large anomalous Hall effect in transport [19–21]. Further growth optimization and chemical potential manipulation led to the recent achievement of the full quantized effect [22–24], albeit at dilution refrigerator temperatures. In two cases [22, 24], an applied magnetic field was necessary to decrease the longitudinal resistivity, presumably to eliminate other conduction channels. The possibilities for these channels include non-chiral edge modes [25], variable-range hopping, or band transport of thermally populated 2D surface or 3D bulk carriers. In contrast, the device measured in Kou *et al.* [23] demonstrates its lowest longitudinal resistance near zero applied field.

In this Letter, we study the QAHE in this regime using material from the same growth, demonstrating the hallmarks of the effect: vanishing longitudinal resistance, precisely quantized Hall resistance that switches sign with magnetization, and direct confirmation of edge transport, all in the absence of an applied field. Where deviations from this ideal behavior occur, we attribute them to thermally-activated carriers whose presence can be fortuitously controlled by demagnetization cooling of some other magnetic system in the sample. The material is 10 quintuple layers of $(Cr_{0.12}Bi_{0.26}Sb_{0.62})_2Te_3$ grown via molecular beam epitaxy and capped with alumina on a semi-insulating GaAs substrate. To avoid possible doping of the film through lithographic processing, following [22] we use a sharp metal tip to scratch the film into a Hall bar shape, and form ohmic contacts by placing indium metal onto each terminal. The region between the voltage leads is 1.1 mm long and 0.45 mm wide (Fig. 1(a)). Four-terminal resistances are measured via standard lock-in amplifier techniques [26] with the sample in
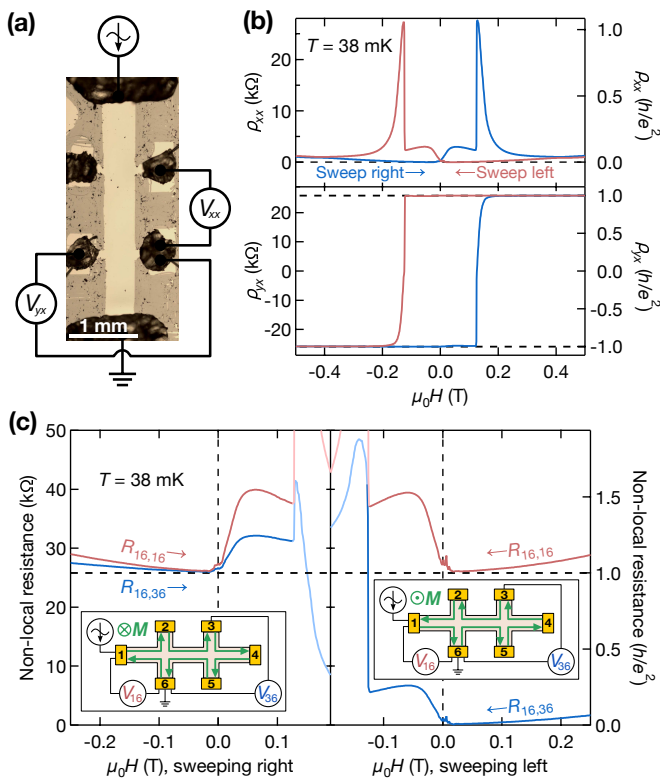
FIG. 1. (Color online) Device demonstrating quantum anomalous Hall effect. (a), Photograph of 10 nm-thick film of $(Cr_{0.12}Bi_{0.26}Sb_{0.62})_2Te_3$ on a GaAs substrate, scratched by hand into Hall bar shape, with indium metal ohmic contacts. Schematic measurement setup included. (b), Longitudinal resistivity ρ_{xx} and transverse resistivity ρ_{yx} of the device at base temperature as a function of the applied magnetic field $\mu_0 H$ in each sweep direction, forming a ferromagnetic hysteresis loop. As the field approaches zero from either starting point, ρ_{yx} reaches its quantized value h/e^2 and ρ_{xx} approaches zero. (c), Non-local and two-terminal measurements verifying edge-dominated transport. The insets show the measurements performed and chirality at each magnetization.

a dilution refrigerator with its mixing chamber cooled to 38 mK. We calibrate the aggregate amplifier gain of the setup using a conventional $\nu = 1$ quantum Hall plateau on a separate high-mobility graphene sample [26].

At base temperature we reproduce the ferromagnetic hysteresis loop measured by the anomalous Hall effect in Kou *et al.* [23] (Fig. 1(b)). The sign of the transverse (Hall) resistivity, ρ_{yx}, reflects the device's magnetization direction, M_z, which we can set to positive ("+1") or negative ("-1") by applying a field $\mu_0 H$ with magnitude greater than the 125 mT coercive field. As we sweep H toward zero, ρ_{yx} reaches its quantized value $\pm h/e^2 \approx \pm 25,813 \; \Omega$ while the longitudinal resistivity ρ_{xx} decreases precipitously (as low as 15 Ω). After crossing zero field, ρ_{xx} increases to a few kΩ before spiking higher at the coercive field as ρ_{yx} changes sign. Both measurements settle toward their quantized values as $|H|$ increases, but

only reach full quantization on the return arm of the hysteresis loop, again just before zero field.

Although the resistivity tensor takes on the expected values, the hysteresis loop does not directly verify that edge conduction dominates in this regime. Non-local measurement configurations, such as that shown schematically in Fig. 1(c), are one way to establish this [35]. In the limit of chiral, ballistic edge transport, the chemical potential along the chirality direction only changes at leads that act as a current sources or drains, as prescribed by Landauer-Büttiker formalism [36] and demonstrated in the QHE [37] (though not explicitly, to date, in the QAHE). For example, while flowing current between adjacent contacts (labelled 1 and 6), the remaining four contacts should maintain the same voltage as either the current source or drain, depending on whether the QAHE chirality is clockwise or counterclockwise, respectively. In Fig. 1(c) we measure the voltage drop from a contact on the opposite side of the device (3) to the drain (6), and plot the resulting three-terminal resistance $R_{16,36}$ compared to the two-terminal value $R_{16,16}$. At negative magnetization (left panel), corresponding to clockwise equilibration, both quantities approach the ballistic value h/e^2, indicating that contact 3 is nearly equilibrated with the source. At the opposite magnetization, where voltages are propagated counterclockwise (right panel), $R_{16,16}$ approaches h/e^2 while $R_{16,36}$ approaches zero due to the equilibration of contact 3 with the drain. Near zero field, the deviations from idealized behavior (in all cases under 200 Ω), likely reflect contact resistances and possibly the presence of extra dissipative helical edge modes [25]. Using one of the remaining contacts in the role of contact 3 results in the same behavior [26].

Returning to four-terminal measurements, we find that the best quantization can be obtained by maintaining the film's magnetization (i.e. keeping $|\mu_0 H|$ smaller than the coercive field) but following the "hysteresis loops" shown in Figure 2(a). Starting from any combination of magnetization and field polarity, sweeping H toward zero suppresses the longitudinal conductivity $\sigma_{xx} = \rho_{xx}/(\rho_{xx}^2 + \rho_{yx}^2)$ to as low as 0.0003 e^2/h while the transverse conductivity $\sigma_{xy} = \rho_{yx}/(\rho_{xx}^2 + \rho_{yx}^2)$ remains quantized to within 0.01% of e^2/h. Passing through zero and then increasing $|H|$ destroys this quantization, which we can recover by waiting at constant field for 80 minutes and then sweeping back toward zero.

These reported conductivity values have undergone one correction for imperfect device geometry. Uneven spacing between the voltage probes of the Hall bar can add a small component of ρ_{xx} to the measured value of ρ_{yx}. (In nonmagnetic samples, this is conventionally corrected by antisymmetrizing ρ_{yx} about zero field.) In a parametric plot of the resistivity data from the same hysteresis loops (Fig. 2(b)), with $|\rho_{yx}|$ along the y-axis and ρ_{xx} along the x-axis, we observe an asymmetry between the two magnetizations. Each branch deviates from a
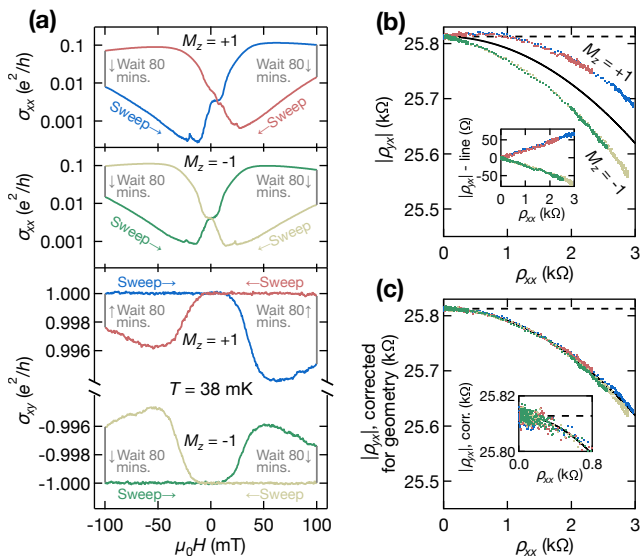
FIG. 2. (Color online) Precise quantization near zero applied field. (a), Longitudinal and transverse conductivities in hysteresis loops over field ranges smaller than the coercive field so as to maintain starting magnetization M_z. When approaching zero field from either starting point, $\sigma_{xy} = e^2/h$ to 0.01% precision while σ_{xx} reaches as low as 0.0002 e^2/h. (b), (c), Resistivities measured during the hysteresis loops, plotted parametrically, both before (b) and after (c) performing a correction for geometry. The inset of (b) shows the linear deviation of the two magnetization branches from a parabolic line, resulting from uneven spacing of the leads. The inset of (c) shows a close-up of the corrected resistivity data, with ρ_{yx} quantized to h/e^2 within 3 Ω whenever $\rho_{xx} < 200$ Ω.

parabolic arc (the expected leading order contribution), with the size of the deviation explicitly verified to grow linearly with ρ_{xx} with a coefficient of 2% (Fig. 2(b), inset). By taking field sweeps at $T = 40$ K, above the film's Curie temperature [23], we obtain an independent but matching measure of this geometric mixing coefficient, which is also verified by a numerical Poisson simulation of current flow [26]. After removing the ρ_{xx} component from ρ_{yx} the data nearly collapse onto a single curve (Fig. 2(c)). In the vicinity of vanishing ρ_{xx}, the parametric plot after this correction demonstrates quantization of ρ_{yx} to within ± 3 Ω (Fig. 2(c), inset).

The system stays on this curve in resistivity space, even during the wait times when ρ_{xx} falls, suggesting that the position along the arc is determined by some parameter other than magnetization or applied field. Temperature is an obvious possibility. We extend the relationship by warming the sample above 100 mK, inducing a large longitudinal conductivity that becomes comparable to e^2/h by 750 mK (Fig. 3). The trajectory of the QAHE in conductivity space during this process has been studied previously, and found to obey the same symmetry laws and renormalization group properties as the QHE [24]. We find reasonable qualitative agreement with calculated [38]

renormalization group flow lines (Fig. 3, gray lines).

To obtain a functional form of the temperature dependence, we plot σ_{xx} versus reciprocal temperature (Fig. 3, inset). Such plots, useful for identifying conduction that is thermally activated over an energy barrier, are commonly used in quantum Hall systems to extract gap sizes [2]. Here, an Arrhenius (exponential) fit holds down to 60 mK, suggesting that the nonzero σ_{xx} represents carriers thermally activated into a surface band. We emphasize that this is not a direct measurement of the size of the exchange gap: with no gate electrode, the chemical potential cannot be tuned to the middle of the surface gap. Furthermore, the fit continues to work well above the extracted energy scale, where describing thermal activation requires use of the Fermi-Dirac distribution as well as knowledge of the system's density of states and mobility as a function of energy [26]. Still, the data show some form of exponential activation suggesting that the nearest band edge is 17 μeV away, as indicated by a 200 mK characteristic temperature in the Arrhenius fit.

At the lowest temperatures, a sample's electron temperature can diverge from the cryostat's base temperature (here, that of the mixing chamber plate). In fact, the wide variation of σ_{xx} in Fig. 2(a) indicates that the temperature may be changing substantially during a hysteresis loop: decreasing as the applied field is swept toward zero, and increasing once the field changes sign and is swept away from zero. We hypothesize that this magnetocaloric effect arises from the demagnetization and remagnetization of some spin system in thermal contact with the sample's electrons. The entropy of these spins can have a large dependence on magnetic field: if the field's magnitude is decreased while the spins are held
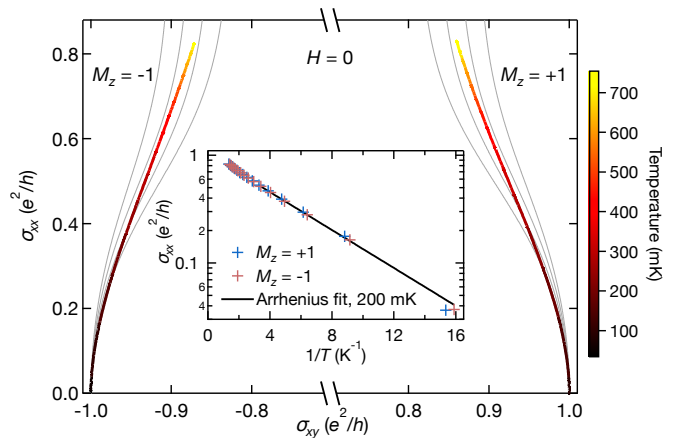

FIG. 3. (Color online) Temperature dependence implying possible thermal activation. Parametric plot of σ_{xx} versus σ_{yx} at each magnetization while increasing temperature, with calculated renormalization group flow lines shown in gray. Inset, an Arrhenius plot of σ_{xx} as a function of inverse temperature, showing roughly exponential dependence. The implied energy scale of the fit is 17 μeV, or 200 mK.
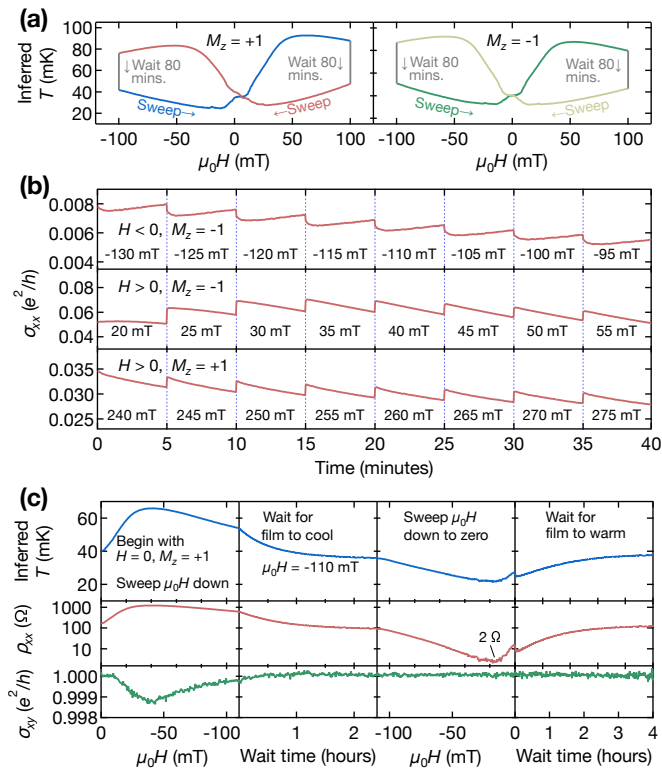
FIG. 4. (Color online) Evidence for demagnetization cooling. (a), Inferred temperature of the TI film, extrapolated using the temperature fit in Figure 3, during the hysteresis loop in Figure 2(a). After a long wait, the temperature approaches the fridge thermometer reading, ~40 mK, whereas sweeping $|H|$ down drives the temperature below 30 mK and sweeping $|H|$ up drives it above 90 mK. (b), Effect of upward field sweep on σ_{xx} in three field/polarity regions, consistent with demagnetization hypothesis. When $H < 0$ (decreasing $|H|$), σ_{xx} decreases when the field changes and creeps back up during a five-minute wait. When $H > 0$ (increasing $|H|$), the opposite occurs regardless of magnetization. (c), A rudimentary demagnetization cycle, involving a slow field sweep to magnetize and a fast field sweep to zero to perform demagnetization cooling. Plotted during this cycle are the inferred temperature, ρ_{xx} (now dropping below 2 Ω), and σ_{xy}, which remains within 0.01% of e^2/h during the last three stages.

at constant temperature, then entropy increases as they depolarize. If, instead, the combined system of electrons and spins is relatively isolated so that total entropy is maintained, its temperature will decrease as the field approaches zero [39]. (Conversely, increasing the field magnitude will lead to sample heating.) This is the principle behind adiabatic demagnetization refrigeration.

To check the reasonability of this hypothesis, we extrapolate the fit in Fig. 3 down to lower temperatures and apply it to the conductance data in Fig. 2(a) to obtain the approximate sample temperature during a hysteresis loop. The result (Fig. 4(a)) implies that the electron temperature after an 80 minute wait at constant field approaches the mixing chamber thermometer reading,

~40 mK. In downward field sweeps the sample drops below 30 mK, substantially below the refrigerator temperature, and in upward sweeps it exceeds 90 mK. (There are also smaller features, presumably heating events, around $|\mu_0 H| = 0$ and 20 mT with unknown origins [26].)

We also test that the sample re-equilibrates with the cryostat between field steps. While sweeping $\mu_0 H$ from negative to positive, we stop for five minutes every 5 mT to allow for partial equilibration. In a field region where H is negative and its magnitude is decreasing (Fig. 4(b), top panel), σ_{xx} decreases during the field step and then creeps back up during the wait time, demonstrating that field has cooled the sample below the cryostat temperature. At positive H the opposite occurs (Fig. 4(b), middle panel) due to the now-warming effect of the field step. The pattern does not change after passing the coercive field and switching the film's magnetization (Fig. 4(b), bottom panel), indicating that only the polarity of the applied field matters, which in turn suggests that the system responsible for these temperature variations is distinct from the ferromagnetism measured in transport.

Although the exact identity of the system responsible for this magnetocaloric effect is otherwise unclear, a naive model of a paramagnet exchanging heat with the electrons qualitatively fits the shape of temperature variation during demagnetization and suggests a Landé g-factor of ~0.15 [26]. We further believe it to be specific to and collocated with the TI sample: the refrigerator's thermometry shows minimal change during the hysteresis loop and, if we pause the loop during demagnetization, σ_{xx} can remain below its equilibrium value for hours. Both details suggest that the TI surface and magnetic system are nearly thermally isolated from the cryostat when driven to their lowest temperatures. Further speculation on the origin of the effect, which has not been observed in materials from other sources, can be found in the Supplementary Information [26].

If we wish to minimize ρ_{xx} or improve quantization of σ_{xy}, an analogy to the traditional adiabatic demagnetization cycle is useful. A slow increase in the field's magnitude followed by a long wait, allowing maximal thermal equilibration along the way, approximates an isothermal magnetization step. Then a fast decrease in field magnitude (though not so fast that the heat load from the magnet sweep becomes relevant), produces adiabatic demagnetization. We plot ρ_{xx}, σ_{xy}, and the inferred temperature during this process in Figure 4(c). Indeed, we drive ρ_{xx} to as low as 2 Ω ($\sigma_{xx} < 0.0001$ e^2/h) and the temperature to 25 mK, with excellent quantization in σ_{xy} along the way. We also include a long wait at the end, demonstrating the long timescale for re-equilibration of ρ_{xx}. Modifying this process to end at a small nonzero applied field, we can even drive ρ_{xx} below 1 Ω [26]. In future studies, adding a gate electrode to optimize the position of the chemical potential in the gap may yield a completely vanishing longitudinal resistance.

Note added.—During preparation of this Letter, we became aware of work by Chang *et al.* that reports a similar degree of quantization in V-doped BiSbTe$_3$ [40].

———————

* To whom correspondence should be addressed; Email: goldhaber-gordon@stanford.edu

[1] K. v. Klitzing, G. Dorda, and M. Pepper, Phys. Rev. Lett. **45**, 494 (1980).

[2] D. C. Tsui, H. L. Stormer, and A. C. Gossard, Phys. Rev. Lett. **48**, 1559 (1982).

[3] R. B. Laughlin, Phys. Rev. B **23**, 5632 (1981).

[4] D. J. Thouless, M. Kohmoto, M. P. Nightingale, and M. den Nijs, Phys. Rev. Lett. **49**, 405 (1982).

[5] K. von Klitzing, Phil. Trans. R. Soc. A **363**, 2203 (2005).

[6] F. D. M. Haldane, Phys. Rev. Lett. **61**, 2015 (1988).

[7] C. L. Kane and E. J. Mele, Phys. Rev. Lett. **95**, 146802 (2005).

[8] B. A. Bernevig, T. L. Hughes, and S.-C. Zhang, Science **314**, 1757 (2006).

[9] M. König, S. Wiedmann, C. Brüne, A. Roth, H. Buhmann, L. W. Molenkamp, X.-L. Qi, and S.-C. Zhang, Science **318**, 766 (2007).

[10] L. Fu, C. L. Kane, and E. J. Mele, Phys. Rev. Lett. **98**, 106803 (2007).

[11] X.-L. Qi, T. L. Hughes, and S.-C. Zhang, Phys. Rev. B **78**, 195424 (2008).

[12] D. Hsieh, Y. Xia, D. Qian, L. Wray, J. H. Dil, F. Meier, J. Osterwalder, L. Patthey, J. G. Checkelsky, N. P. Ong, A. V. Fedorov, H. Lin, A. Bansil, D. Grauer, Y. S. Hor, R. J. Cava, and M. Z. Hasan, Nature **460**, 1101 (2009).

[13] M. Z. Hasan and C. L. Kane, Rev. Mod. Phys. **82**, 3045 (2010).

[14] X.-L. Qi and S.-C. Zhang, Rev. Mod. Phys. **83**, 1057 (2011).

[15] R. Yu, W. Zhang, H.-J. Zhang, S.-C. Zhang, X. Dai, and Z. Fang, Science **329**, 61 (2010).

[16] K. Nomura and N. Nagaosa, Phys. Rev. Lett. **106**, 166802 (2011).

[17] Y. L. Chen, J.-H. Chu, J. G. Analytis, Z. K. Liu, K. Igarashi, H.-H. Kuo, X. L. Qi, S. K. Mo, R. G. Moore, D. H. Lu, M. Hashimoto, T. Sasagawa, S. C. Zhang, I. R. Fisher, Z. Hussain, and Z. X. Shen, Science **329**, 659 (2010).

[18] J. Wang, B. Lian, H. Zhang, Y. Xu, and S.-C. Zhang, Phys. Rev. Lett. **111**, 136801 (2013).

[19] J. G. Checkelsky, J. Ye, Y. Onose, Y. Iwasa, and Y. Tokura, Nat. Phys. **8**, 729 (2012).

[20] C.-Z. Chang, J. Zhang, M. Liu, Z. Zhang, X. Feng, K. Li, L.-L. Wang, X. Chen, X. Dai, Z. Fang, X.-L. Qi, S.-C. Zhang, Y. Wang, K. He, X.-C. Ma, and Q.-K. Xue, Adv. Mater. **25**, 1065 (2013).

[21] X. Kou, M. Lang, Y. Fan, Y. Jiang, T. Nie, J. Zhang, W. Jiang, Y. Wang, Y. Yao, L. He, and K. L. Wang, ACS Nano **7**, 9205 (2013).

[22] C.-Z. Chang, J. Zhang, X. Feng, J. Shen, Z. Zhang, M. Guo, K. Li, Y. Ou, P. Wei, L.-L. Wang, Z.-Q. Ji, Y. Feng, S. Ji, X. Chen, J. Jia, X. Dai, Z. Fang, S.-C. Zhang, K. He, Y. Wang, L. Lu, X.-C. Ma, and Q.-K. Xue, Science **340**, 167 (2013).

[23] X. Kou, S.-T. Guo, Y. Fan, L. Pan, M. Lang, Y. Jiang, Q. Shao, T. Nie, K. Murata, J. Tang, Y. Wang, L. He, T.-K. Lee, W.-L. Lee, and K. L. Wang, Phys. Rev. Lett. **113**, 137201 (2014).

[24] J. G. Checkelsky, R. Yoshimi, A. Tsukazaki, K. S. Takahashi, Y. Kozuka, J. Falson, M. Kawasaki, and Y. Tokura, Nat. Phys. **10**, 731 (2014).

[25] J. Wang, B. Lian, H. Zhang, and S.-C. Zhang, Phys. Rev. Lett. **111**, 086803 (2013).

[26] See Supplemental Material [url], which includes Refs. [27–34].

[27] L. He, X. Kou, M. Lang, E. S. Choi, Y. Jiang, T. Nie, W. Jiang, Y. Fan, Y. Wang, F. Xiu, and K. L. Wang, Sci. Rep. **3** (2013).

[28] M. Lang, L. He, F. Xiu, X. Yu, J. Tang, Y. Wang, X. Kou, W. Jiang, A. V. Fedorov, and K. L. Wang, ACS Nano **6**, 295 (2012).

[29] F. P. Milliken, J. R. Rozen, G. A. Keefe, and R. H. Koch, Rev. Sci. Instrum. **78**, 024701 (2007).

[30] F. Fischer and M. Grayson, J. Appl. Phys. **98**, 013710 (2005).

[31] P. L. Gammel, D. J. Bishop, J. P. Eisenstein, J. H. English, A. C. Gossard, R. Ruel, and H. L. Stormer, Phys. Rev. B **38**, 10128 (1988).

[32] C.-Z. Chang, P. Tang, Y.-L. Wang, X. Feng, K. Li, Z. Zhang, Y. Wang, L.-L. Wang, X. Chen, C. Liu, W. Duan, K. He, X.-C. Ma, and Q.-K. Xue, Phys. Rev. Lett. **112**, 056801 (2014).

[33] K. Elliott, R. T. Chen, S. G. Greenbaum, and R. J. Wagner, Appl. Phys. Lett. **44**, 907 (1984).

[34] J. S. Blakemore, J. Appl. Phys. **53**, R123 (1982).

[35] A. Roth, C. Brüne, H. Buhmann, L. W. Molenkamp, J. Maciejko, X.-L. Qi, and S.-C. Zhang, Science **325**, 294 (2009).

[36] M. Büttiker, Phys. Rev. B **38**, 9375 (1988).

[37] C. Beenakker and H. van Houten, in *Semiconductor Het-*

erostructures and Nanostructures, Solid State Physics, Vol. 44, edited by H. Ehrenreich and D. Turnbull (Academic Press, 1991) pp. 1 – 228.

[38] B. P. Dolan, Nucl. Phys. B **554**, 487 (1999).

[39] V. K. Pecharsky, K. A. Gschneidner, A. O. Pecharsky, and A. M. Tishin, Phys. Rev. B **64**, 144406 (2001).

[40] C.-Z. Chang, W. Zhao, D. Y. Kim, H. Zhang, B. A. Assaf, D. Heiman, S.-C. Zhang, C. Liu, M. H. W. Chan, and J. S. Moodera, ArXiv e-prints (2014), arXiv:1412.3758 [cond-mat.mtrl-sci].